Numerical and experimental studies of a distributed Bragg reflector laser

V. Z. Tronciu
Department of Physics,
Technical University of Moldova,
Chisinau, Republic of Moldova
vasile.tronciu@fiz.utm.md

H. Wenzel and A. Knigge
Ferdinand-Braun-Institut,
Leibniz-Insitut für Höchstfrequenztechnik,
Berlin, Germany

M. Radziunas
Laser dynamics group,
Weierstrass Institute,
Berlin, Germany

M. Reggentin and J. Wiedmann
eagleyard Photonics GmbH,
Berlin, Germany

***Abstract*—We report in this paper theoretical and experimental results on the dynamical properties of a distributed Bragg reflector (DBR) semiconductor lasers. Using the traveling wave equation model, we show that a proper choice of coupling coefficient and front facet reflectivity allows an optimization of the laser operation, such that for a wide range of currents injected into the active region the laser emits a continuous-wave beam. The numerical results are in a qualitative agreement with measured characteristics.**

***Index Terms*— distributed Bragg reflector (DBR), CW operation, instabilities**

I. Introduction

Applications such as high precision metrology, Raman spectroscopy, interferometry, and holography require red-emitting lasers with small spectral linewidth and good beam quality. To meet these requirements with diode lasers, Bragg gratings for wavelength stabilization have to be monolithically integrated into the cavity [1]. Whereas in a distributed feedback (DFB) laser the grating extends over the whole cavity, in a distributed Bragg (DBR) laser the grating is implemented only in a part of the cavity. Thus, DBR lasers consist always of at least two sections - an active section and a passive section. If the active layer in a DBR laser extends over the whole cavity, the DBR section can act like a saturable absorber which is known to cause a dynamic unstable behavior [2], [3], [4].

Recently we investigated the performance of a DBR laser emitting around 1060 nm by numerical simulations based on a traveling wave model [5]. The mode jumps occurring for increasing or decreasing injection current could be well explained by a modal analysis [5], [6]. The multimode transitions regions around the jumps which are related to dynamic instabilities [7] hinder the utilization of DBR lasers for the above mentioned applications which need stable single-longitudinal mode operation over a sufficiently large range of parameters such as current and temperature.

In this paper we study the impact of device and material parameters such as coupling coefficient of the grating and facet reflectivity on the dynamic instabilities of a DBR laser emitting around 660 nm. The paper is organized as follows. The device structure and mathematical model are presented in Section II. The theoretical and experimental results are described in Section III. Finally, some conclusions are drawn in Section IV.

II. Laser structure and theoretical model

The DBR laser under study is similar to the device reported in [8]. The vertical structure grown on n-GaAs substrate consists of n-AlInP cladding, n-AlInGaP confinement, active, p-AlInGaP confinement and p-AlGaAs cladding layers. The complete layer structure including the active layer which is a compressively strained single InGaP quantum well extends over the whole cavity. Lateral optical confinement is provided by a ridge waveguide with a ridge width of 5 μm. Wavelength stabilization is achieved by a 10th order surface grating etched into the p-AlGaAs cladding layer of the ridge of the DBR section. The lengths of active and DBR sections are $l_A = 1500\,\mu\text{m}$ and $l_{DBR} = 500\,\mu\text{m}$, respectively. A pictorial schematic of the DBR laser is given in Fig. 1.

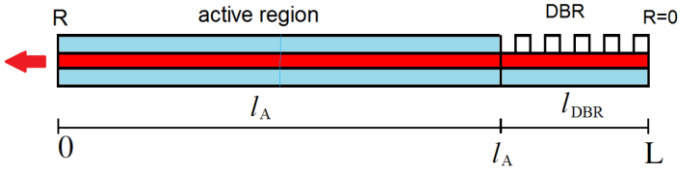

Fig. 1 Scheme of a DBR device consisting of active region coupled with a DBR section.

To simulate the dynamics of the DBR laser we use a model based on the 1 (time)+1 (space) dimensional traveling wave (TW) equations for the slowly varying complex amplitudes

$E^+(z,t)$ and $E^-(z,t)$ of the counter-propagating optical fields within each section of the laser [6], [9]

$$\frac{n_g}{c_0}\frac{\partial}{\partial t}E^{\pm} = \left[\mp\frac{\partial}{\partial z} - i\Delta\beta(N,I)\right]E^{\pm} - i\kappa E^{\mp} + F_{sp}^{\pm} \quad (1)$$

where c_0 is the speed of light in vacuum, F_{sp} is the stochastic contribution of spontaneous emission in the active section, n_g is the group index, κ is the field coupling coefficient due to the Bragg gratings, whereas the scaling of the fields $E^{\pm}$ is such that $|E|^2 = |E^+|^2 + |E^-|^2$ is the local photon density. Eqs. (1) are supplemented by the usual reflective boundary conditions. The relative propagation factor in each section is given by

$$\Delta\beta = \delta_0 - i\frac{\alpha_0}{2} + k_0[\Delta n_N(N) + \Delta n_T(I)] + i\frac{g(N)-D}{2} \quad (2)$$

where δ_0 is a static detuning, α_0 the internal optical losses and $k_0 = 2\pi/\lambda_0$ with λ_0 being the reference wavelength. The modal peak gain is assumed to depend linearly on the carrier density

$$g(N) = \frac{\Gamma g'(N - N_{tr})}{1 + \varepsilon_g |E|^2} \quad (3)$$

where Γ is the optical confinement factor, g' the differential gain, N_{tr} the transparency carrier density and ε_g is the gain compression factor.

The change of the effective index with carrier density is modeled by the square root function [7]

$$\Delta n_N = \tilde{\alpha}_H \frac{\Gamma g'}{k_0}\sqrt{\frac{N}{N_{tr}}} \quad (4)$$

Note that the proportionality factor $\tilde{\alpha}_H$ in (4) differs from the well known linewidth enhancement or Henry factor α_H.

The function $\Delta n_T(I)$ describes the change of the effective index in a laser section due to self- and cross-heating induced by the injection current [5], [7] and is the major factor implying transitions between longitudinal modes when the injection current is varied.

In this paper we neglect cross-heating effects for simplicity, so that within each section the relation

$$\Delta n_T = \frac{n_g}{\lambda_0}\nu I. \quad (5)$$

holds. The linear operator

$$DE^{\pm} = \bar{g}(E^{\pm} - P^{\pm}), \quad \frac{\partial}{\partial t}P^{\pm} = \bar{\gamma}(E^{\pm} - P^{\pm}) + i\bar{\omega}P^{\pm} \quad (6)$$

is used to model the dispersion of the gain by a Lorentzian approximation [10].

The rate equation for the carrier density $N(z,t)$ in each section reads

$$\frac{\partial}{\partial t}N = \frac{I}{edWl_A} + \frac{U_F'}{edr_s}(\bar{N} - N) - \left(\frac{N}{\tau} + BN^2 + CN^3\right) - \frac{c_0}{n_g}\Re\sum_{\nu=\pm}E^{\nu *}[g(N) - D]E^{\nu} \quad (7)$$

where d and W are the thickness and the widths, respectively, of the active layer and B and C are the recombination parameters.

The second term on the right hand side describes the self-distribution of the injected current due to a non-vanishing series resistance r_s [11] with U_F' being the derivative of the Fermi level separation and N is the average carrier density in the section.

For a detailed description of the remaining model equations and parameters we refer to [6], [9].

III. Theoretical and Experimental Results

In what follows we present numerical results obtained using the TW model (1)-(6). Figure 2 shows the experimentally (black dotted) measured and numerically calculated (red solid) dependence of the optical output power at the front facet (located at z = 0) versus the current injected into the active section of the DBR laser shown in Fig. 1. Due to the fact that the TWA model neglects lateral effects the current has been multiplied by a factor of 1.4 to account for lateral current spreading and diffusion, which increase the effective contact width. The factor has been determined by comparing the transparency currents of ridge waveguide lasers and broad area lasers where the lateral effects can be neglected.

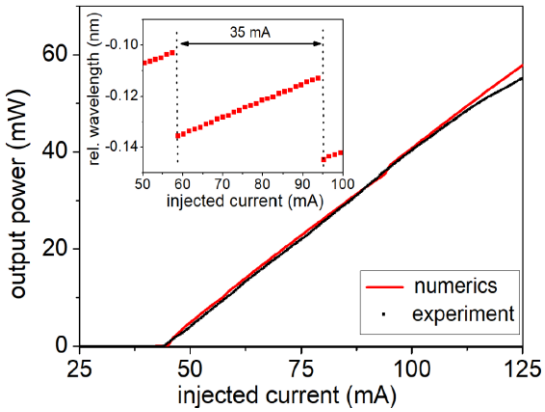

Fig. 2. Calculated (red line) and measured (black dots) power–current characteristics. Insert: Calculated lasing wavelength versus current.

The characteristics show a threshold current of 45 mA both in theory and experiment. The power-current characteristic is nearly linear with a slope efficiency of 0.73 W/A. We mention that the experimental investigations were performed at a temperature of 22 °C. The insert shows the lasing wavelength as a function of the injection current. One can observe a current period of the mode jumps of 35 mA which is in a good agreement with that of the experiment shown in Fig. 3a.

Figure 3a shows a pseudo-color mapping of the lasing wavelength recorded with a wavemeter in dependence on the temperature of the diode laser and the current injected into the active section. The current step is 2 mA. For a given temperature, in the current range investigated there are 2 mode jumps separating areas A, B and C with single mode

operation. At a temperature of 24 °C the current period of the mode jumps (height of area B) is 35 mA. The dark areas indicate regions where the wavemeter was not able to determine a unique wavelength. The dark area named D corresponds to subthreshold operation. The dark area U between currents of 80 mA and 95 mA ranging up to temperatures of about 30 °C shown below in Fig. 3a indicates a dynamic unstable region. With increasing temperature the lasing threshold rises and only continuous-wave (CW) operation is present once the laser is switched on, i.e. the region of dynamic instability U disappears.

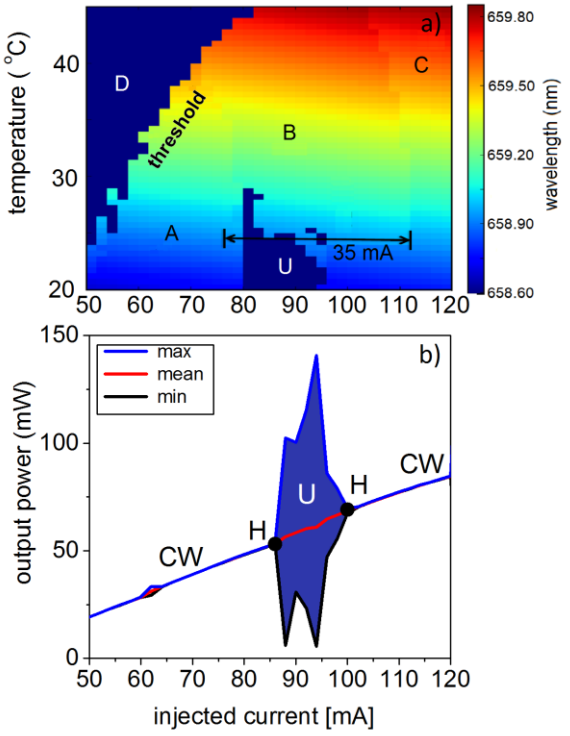

Fig. 3 a) Experimental pseudo-color mapping of the lasing wavelength of a DBR laser in dependence on mount temperature and injection current. b) Simulated non-stationary state: maximal, minimal and mean power. CW: continue waves. U: unstable region. H: Hopf bifurcation.

Fig. 3 b) represents an evolution of the simulated values of the local maxima, minima and mean values of the emitted power if the injection current is increased from 50 to 120 mA. For I = 50 mA stable CW operation is observed. The unstable region "SP" begins when a bifurcation (marked by a circle) is reached. After the bifurcation the amplitudes of the self-pulsations increase and reach a maximum and then decline eventually disappearing at another bifurcation. Both bifurcations are of supercritical Hopf type.

In the next step, we investigate the influence of some device parameters on the laser behavior. First, we consider the influence of the coupling coefficient κ which is non-vanishing only in the DBR section. Fig. 4 shows the laser behavior for different values of κ. For κ=20 cm^{-1}, see Fig. 4a), only few jumps of the emission intensity can be observed when varying the injection current. The lasing between these few jumps is of the stable CW type. By increasing the coefficient κ to 30 cm^{-1} and performing the same current-varying simulations one can observe a small increase of the unstable lasing regions in the close vicinity of the state transitions, see gray regions in Fig. 4 b). For the standard value of the coupling coefficient κ=40 cm^{-1}, an unstable lasing region is found in the current range between 85 and 110 mA, which is denoted by the gray color in Fig. 3 b). We note that a similar unstable region was observed in the experiments (see Fig. 3a), so as mentioned above, this value was used in our calculations. A further increase of κ leads to a more pronounced evidence of unstable lasing in the current-varying simulations, see Fig. 4c).

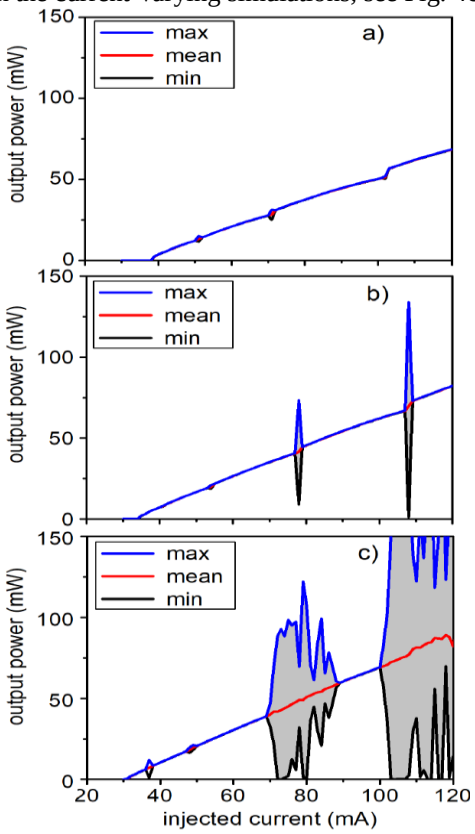

Fig. 4 The influence of the coupling parameter κ on the on the power current characteristics: a) κ = 20 cm^{-1}, b) κ = 30 cm^{-1}, c) κ = 50 cm^{-1}. Gray regions: unstable. Blue line maximum, red line mean, and black line minimum output power.

Another parameter with impact on the output characteristics of the DBR laser worth to be studied is the reflectivity of the front facet because it can be easily varied by employing an appropriate coating. The standard value of the front facet reflectivity is R_f = 0.3. Figure 5 a) shows again the dependence of output power on the injection current for this value of R_f. The choice of a smaller value of R_f leads to an increase of the threshold current and to a shift of the unstable region to higher currents, see Fig. 5 b). In the extreme case of R_f = 0.01, CW lasing is dominating and there is no significant unstable lasing region within the considered injected current range, see panel c) of the same figure. It should be noted, however, that the associated strong increase of the threshold current could

prevent lasing at all, because it could result in increased minority leakage currents and free-carrier absorption as well as increased self-heating, not accounted for in the model. Nevertheless, the results reveal that a diminution of the unstable regimes can be achieved by proper optimization of the front facet reflectivity and of the coupling coefficient.

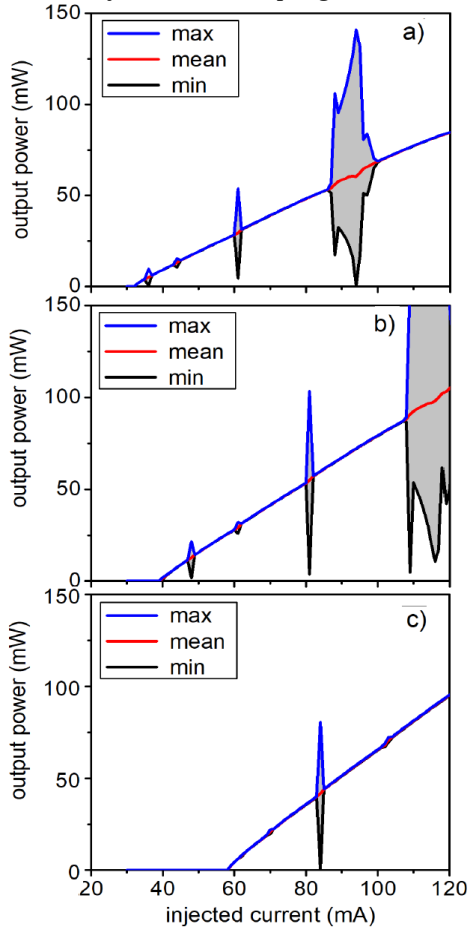

Fig. 5 The influence of front facet reflectivity on the power current characteristics for a) $R_f = 0.3$, b) $R_f = 0.1$, c) $R_f = 0.01$. Notations are as in Fig. 4.

IV. Conclusions

We have carried out experimental and theoretical investigations of the dynamics of a DBR semiconductor laser. Operation of the laser has been described using the traveling wave model adapted to the specific case of a semiconductor laser with DBR section. Both simulations and experiments show the presence of unstable regions in the domain of different parameters. It was found that the main device and material parameters play a major role in the laser dynamics. In particular, we have found that the front facet reflectivity and the coupling coefficient have to be carefully chosen to obtain a more pronounced stable CW operation of the DBR laser within a wide region of injection currents. We believe that our work provides a good basis for more detailed investigations of stable operating DBR lasers.

Acknowledgment

The work of V. Tronciu has been supported by the Technical University of Moldova projects 14.02.116F/34S and 16.80012.02.27F. The authors are indebted to J. Pohl and J. Fricke (Ferdinand-Braun-Institut) for expitaxial growth and processing, respectively. The support of C. Noelleke (TOPTICA Photonics AG) for wavelength mapping measurements is gratefully acknowledged.

References

[1] P. Crump, O. Brox, F. Bugge, J. Fricke, C. Schultz, M. Spreemann, B. Sumpf, H. Wenzel, G. Erbert, "High power, high efficiency monolithic edge–emitting GaAs–based lasers with narrow spectral widths", in: Coleman, J. J., Bryce, A. C. Jagadish, C. (Eds.): Advances in Semiconductor Lasers (Academic Press, 2012), pp. 49–91

[2] M. Yamada, "A theoretical analysis of self-sustained pulsation phenomena in narrow-stripe semiconductor lasers", IEEE J. Quantum Electron., 1993, 29, (5), pp. 1330–1336

[3] C. R. Mirasso, G. H. Van Tartwijk, E. Hernandez-Garcia, D. Lenstra, S. Lynch, P. Landais, P. Phelan, J. O'Gorman, M. San Miguel, W. Elsasser, "Self-pulsating semiconductor lasers: theory and experiment", IEEE J. Quantum Electron., 1999, 35, (5), pp. 764–77

[4] V. Tronciu, M. Yamada, T. Ohno, S. Ito, T. Kawakami, M. Taneya, "Selfpulsation in an InGaN laser – theory and experiment", IEEE J. Quantum Electron., 2003, 39, (12), pp. 1509–1514

[5] M. Radziunas, K. H. Hasler, B. Sumpf, T. Q. Tien, H. Wenzel, "Mode transitions in distributed Bragg reflector semiconductor lasers: Experiments, simulations and analysis", J. Phys. B: Atomic, Molecular and Optical Physics, 2011, 44,, p. 105401

[6] M. Radziunas, H. J. Wünsche, "Multisection lasers: longitudinal modes and their dynamics", in: J. Piprek (Ed.), Optoelectronic Devices, Springer: New York, 2005, pp. 121–150.

[7] M. Spreemann, M. Lichtner, M. Radziunas, U. Bandelow, H. Wenzel, "Measurement and simulation of distributed–feedback tapered master–oscillator power amplifiers", IEEE J. Quantum Electron., 2009, 45, (6), pp. 609–616

[8] D. Feise, W. John, F. Bugge, G. Blume, T. Hassoun, J. Fricke, K. Paschke, G. Erbert, "96 mW longitudinal single mode red-emitting distributed Bragg reflectorridge waveguide laser with tenth order surface gratings", Opt. Lett., 2012, 37, pp. 1532–1534

[9] M. Radziunas, "Traveling wave modeling of nonlinear dynamics in multisection laser diodes", in: J. Piprek (Ed.), Handbook of Optoelectronic Device Modeling and Simulation: Lasers, Modulators, Photodetectors, Solar Cells, and Numerical Methods, Vol. 2, CRC Press, 2017, Ch. 31.

[10] C. Ning, R. Indik, J. Moloney, "Effective Bloch equations for semiconductorlasers and amplifiers", IEEE J. Quantum Electron., 1997, 33, (9), pp. 1543–1550

[11] U. Bandelow, H. Wenzel, H. J. Wünsche, "Influence of inhomogeneous injection on sidemode suppression in strongly coupled DFB semiconductor lasers", Electron. Lett., 1992, 28, (14), pp. 1324–1326